Applied Physics Express 6 (2013) 112701
http://dx.doi.org/10.7567/APEX.6.112701

Evolution of Femtosecond Laser-Induced Surface Ripples on Lithium Niobate Crystal Surfaces

Hisashi Shimizu[1], Go Obara[1], Mitsuhiro Terakawa[1], Eric Mazur[2], and Minoru Obara[1]*

[1]School of Integrated Design Engineering, Keio University, Yokohama 223-8522, Japan
[2]Department of Physics, Harvard University, Cambridge, MA 02138, U.S.A.
E-mail: obara@obara.elec.keio.ac.jp

Received August 30, 2013; accepted September 25, 2013; published online October 11, 2013

We fabricated periodic ripple structures on the surface of a lithium niobate crystal by irradiation with femtosecond laser pulses and observed the evolution of these structures under irradiation with successive laser pulses. After just a few laser pulses we observed nanorod-shaped craters, aligned with each other but randomly distributed over the surface. The nanocraters are caused by nanoablation at defects in the crystal surface. With increasing pulse number, side-lobed nanocraters appear and light scattered from the initial nanorod-shaped craters at the crystal surface interferes with the incident light, causing the formation of periodic structures.

Irradiation of a material surface with multiple femtosecond laser pulses of moderate fluence enables the formation of ripple-like surface structures of a periodicity close to or shorter than the irradiation wavelength. Many researchers have discussed the underlying physics for the formation processes of periodic structures[1–6] in metals,[4,7] semiconductors,[5–10] and wide-bandgap dielectrics.[11,12] These structures are called laser-induced periodic surface structures (LIPSSs), and have attracted much attention because of the advantages of high-throughput fabrication of nanoscale structures by a simple, dry process. Applications of LIPSSs include enhancement of thin-film adhesion,[13] structural color,[14] and cell biology.[15] LIPSSs are classified into two groups according to the periodicity of ripples; low-spatial-frequency LIPSS (LSFL), and high-spatial-frequency LIPSS (HSFL). LSFL of periods near the irradiation wavelength have been observed on the surface of metals and semiconductors.[4–9] On the surface of dielectrics, HSFL formation has been reported with periodicities ranging from $\lambda/2n$ to $\lambda/6n$,[11,12] where λ is the incident laser wavelength in vacuum and n is the refractive index. For LSFL, ripple formation is attributed to interference of a surface plasmon wave with the incident light.[16,17]

On the other hand, HSFL formation has been attributed to second harmonic generation[10,18] and a change in the refractive index.[19] Recent work on HSFL formation on the surface of fused silica has shown a transition from a grooved structure to HSFL.[20] Incubation effects related to the spatial profile of the incident laser beam generate local maxima in the optical intensity profile, resulting in HSFL.[20] However, most hypotheses explain only individual experiments: a more fundamental theory is necessary to explain the HSFL formation.

Lithium niobate ($LiNbO_3$, LN) crystals have been used in optical circuits, optical modulators, and optical frequency converters. There are several reports of femtosecond laser processing of crystalline LN, including laser-written waveguides[21] and ripple formation by a tightly focused femtosecond laser.[12]

In this paper, we present observations of the onset of LIPSSs at the surface of a transparent lithium niobate crystal. After irradiation with just a few femtosecond laser pulses we observe the formation of nanorod-shaped craters that are distributed randomly on the surface. The formation of these craters is mainly due to local nanoablation, stemming from avalanche ionization following electron excitation at surface defects. We use a three-dimensional (3D) finite-difference time-domain (FDTD) method to explain the onset of ripple formation.

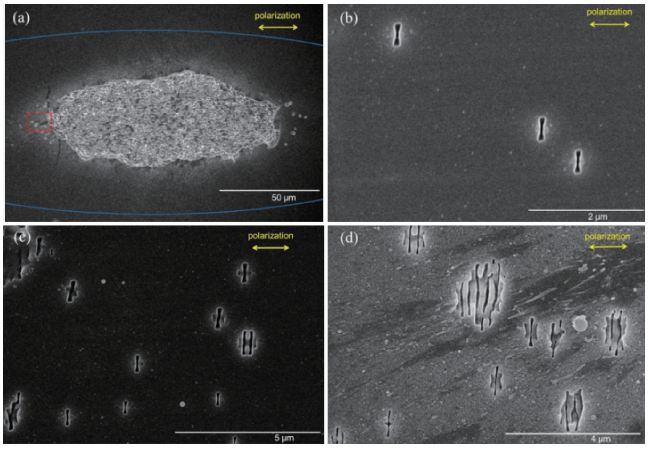

Fig. 1. SEM images of $LiNbO_3$ (LN) crystal surface after the femtosecond laser irradiation. The periodicity of the ripple structures is about 150 nm. Yellow arrows show the linear polarization direction of the incident laser. (a) Whole view of the ablated area. The blue ellipse shows the laser spot ($1/e^2$ of peak laser intensity) with dimensions of $90 \times 300\,\mu m^2$. Note that in Fig. 2 the beam spot is circular. We observed the red square area. The magnified SEM images are shown in Figs. 1(b), 1(c), and 1(d). (b) Number of pulses $N = 11$, and irradiation fluence $F = 470\,mJ/cm^2$, (c) $N = 11$, $F = 610\,mJ/cm^2$, (d) $N = 22$, $F = 540\,mJ/cm^2$.

We irradiated the surface of a 500-μm-thick LN crystal at a normal incidence with femtosecond laser pulses (Libra, Coherent) of 80 fs duration at a central wavelength of 800 nm and a repetition rate of 1 kHz. The laser was loosely focused by a plano-convex lens (200 mm focal length) on z-cut LN (ordinary-ray refractive index $n_o = 2.25$, extraordinary-ray refractive index $n_e = 2.17$ at $\lambda = 800\,nm$[22]). The laser fluence was kept below the ablation threshold for a single pulse ($1.8\,J/cm^2$ at 800 nm and 130 fs[23]).

Figure 1 shows scanning electron microscopy (SEM) images of the LN crystal surface after laser irradiation. A complete view of the ablated area defined by the laser beam is shown in Fig. 1(a). The blue ellipse shows the dimensions of the irradiated area ($90 \times 300\,\mu m^2$, defined by $1/e^2$ of the peak laser intensity at the surface). After irradiation with 11 pulses, nanorod-shaped craters appear randomly in the

irradiated area [Fig. 1(b)]. The nanorod-shaped craters are all aligned perpendicular to the incident polarization. The formation of nanorod-shaped craters with linear polarization irradiation substantiates the existence of straight-line structured stacking faults.

As the incident laser fluence is increased, side-lobed craters appear on both sides of the nanorod-shaped craters [Figs. 1(b) and 1(c)]. The formation of the nanorod-shaped and side-lobed craters depends not only on the fluence but also on the number of pulses. As the number of laser pulses is increased, the side-lobed craters are formed at lower fluences, resulting in the growth of ripple structures corresponding to HSFL [Fig. 1(d)].

The distance between the center of the nanorod-shaped crater and the side-lobed craters ranges from 90 to 200 nm [Figs. 1(c) and 1(d)]. The first pulses ablate a nanorod-shaped crater on the crystal surface and subsequent pulses interfere with the wave scattered from the nanorod-shaped craters forming the side-lobed craters. In 1973, Bloembergen reported that defects, including cracks, pores, and absorbing inclusions, reduce the laser-induced damage threshold of transparent optical materials.[24] Inclusions and cracks with characteristic dimensions of less than 10 nm do not lower the breakdown threshold appreciably. The nanocraters we observed can be attributed to ablation resulting from absorption of the incident radiation at defects in the LN crystal. The defects include stacking faults and point defects, which occur naturally during the crystal growth. The effects of a variety of defects on the optical properties of LN crystals were discussed in the 1990s.[25] However, present-day LN crystals contain only trace defects, including metal ions such as Cr, Fe, Ni, and Cu, which form shallow defect levels in the LN band structure and cause the absorption of visible and near-infrared light.[26] The LN crystals used in our experiment nominally contain minute amounts of metal defects (Fe < 1.0, Cr < 0.1, Ni < 0.1, Cu < 0.1 ppm). At a concentration of 1 ppm, metal ion defects are separated on average by 380 nm, assuming that the distance between Li and Nb atoms in LN is 0.3765 nm. While these metallic impurities may not scatter strongly, the stacking faults contribute to the local electron excitation, and the locally excited electrons seed an avalanche ionization that results in ablation. The random distribution of nanorod-shaped craters we observe may reflect the random distribution of stacking faults.

In addition to the linear-polarization experiment described above, we also irradiated the LN crystal in a separate experiment with circularly polarized femtosecond laser pulses. The SEM image of the resulting surface of the LN crystal is shown in Fig. 2. Under circularly polarized laser irradiation, the nanorod-shaped craters do not align in the same direction [Fig. 2(b)], and the shape of the craters is not identical to that obtained with linear polarization irradiation [Fig. 1(b)]. The formation of nanorod-like craters with circularly polarized irradiation also suggests the role of stacking faults as an initial scatterer.

The stacking faults are straight-line structures and are formed during the growth of the LN crystal.[27] The stacking faults have a different optical refractive index from the surrounding crystal, resulting in the scattering of the incident light. The difference in the refractive index behaves as a

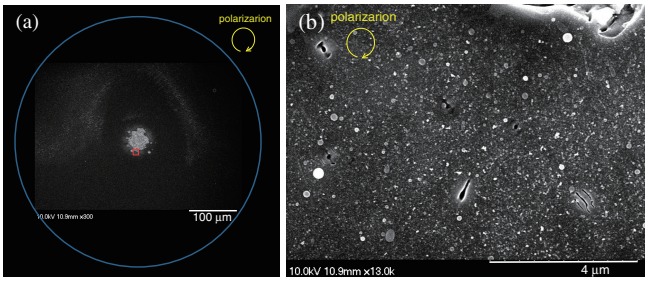

Fig. 2. SEM images of LN crystal surface after the circularly polarized femtosecond laser irradiation. Yellow arrows show the circular polarization direction. (a) Whole view of the ablated area. The blue circle shows the laser spot ($1/e^2$ of peak laser intensity). The red square shows the magnified area in Fig. 2(b). The beam spot diameter is 500 μm. (b): Number of pulses $N = 20$, $F = 1.1\,\mathrm{J/cm^2}$.

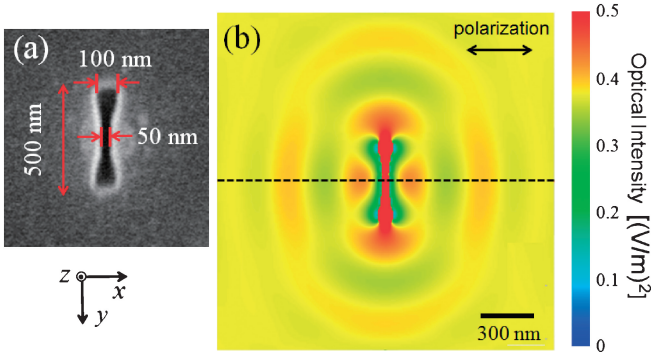

Fig. 3. SEM image (a) and optical intensity distribution close to a nanorod-shaped crater calculated by FDTD simulation (b). The incident electric field strength is set to 1 V/m.

far-field wave source via Mie scattering.[28,29] Due to their different refractive index, the stacking faults scatter the perpendicular component of the circularly polarized incident laser pulse, forming an interference intensity pattern. Therefore, even with circularly polarized light, nanorod-shaped craters can be formed, albeit less efficiently, and defects result in ripple formation after the initial few pulses.

In order to elucidate the scattering process for ripple formation close to the nanorod-shaped craters, we modeled the optical intensity distribution using a 3D-FDTD algorithm. A linearly polarized wave strikes the LN surface at normal incidence and irradiates the surface uniformly. The incident electric field is taken to be 1 V/m and we used $n = 2.17 + 0i$ at 800 nm for the LN crystal.[22] LN is a wide-bandgap material ($E_g = 4\,\mathrm{eV}$) so we can assume that the electron density in the conduction band does not increase during laser irradiation. Figure 3 shows the steady-state intensity distribution at a depth $z = -5$ nm below the crystal surface 22 fs after irradiation with an 800 nm femtosecond laser pulse. We chose to analyze the field distribution just below the surface ($z = -5$ nm) because the material at that depth plays a more important role in the ablation process than the surface.

The simulation agrees well with the experimental result, showing strong enhancement of the optical intensity at both ends of the nanorod-shaped crater. The intensity

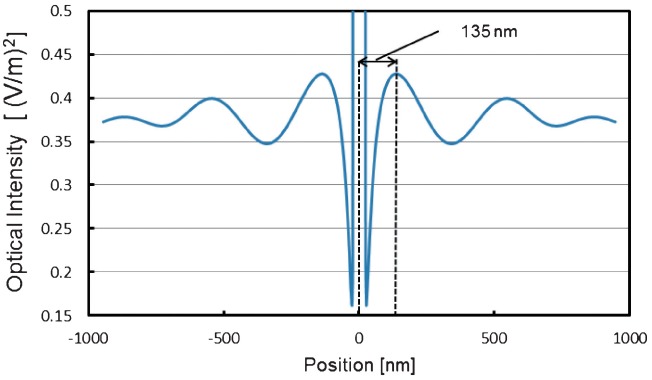

Fig. 4. Optical intensity along the dashed line in Fig. 3 calculated by FDTD simulation. The distance from the center of the nanorod-shaped crater to the first peak of the optical intensity is 135 nm.

enhancement shown in Fig. 3(b), which is produced by the interference of the scattered wave from the nanorod crater and the incident laser, is likely to be responsible for the formation of the side-lobed craters. With increasing number of laser pulses, the nanocraters extend to form periodic ripples parallel to the original crater. Figure 4 shows the intensity distribution at $z = -5$ nm along the dashed line in Fig. 3. At a wavelength of 800 nm ($h\nu = 1.55$ eV) a three-photon process is necessary to excite carriers across the bandgap of LN ($E_g = 4$ eV). The ablation and the modification occur at the area where the value of the enhanced optical intensity exceeds the ablation threshold for nanocrater formation. Experimental distance between the center of the nanorod-shaped crater and the side-lobed craters ranged from 90 to 200 nm [Figs. 1(c) and 1(d)]. By FDTD simulation, the distance is calculated as 135 nm. The simulation explains well the observations of the evolution of high-spatial-frequency LIPSS formation.

In conclusion, we observed the evolution of high-spatial-frequency LIPSS formation at the surface of a LN crystal. After irradiation of a few pulses, nanorod-shaped craters appear randomly on the surface. The formation of the nanocraters is mainly due to local nanoablation, originating from stacking faults in the crystal. Subsequent incident pulses turn the nanorod-shaped craters into side-lobed craters. We used 3D-FDTD modeling to explain the onset of ripple formation and the pulse number evolution of the periodic structures.

Acknowledgments This study was supported in part by a Grant-in-Aid for Scientific Research (B-23360161) from the Ministry of Education, Culture, Sports, Science and Technology (MEXT), Japan. The authors are grateful to K. Hirano for his assistance. G. Obara is grateful for the JSPS Fellowship for Young Scientists.

1) J. E. Sipe, J. F. Young, J. S. Preston, and H. M. van Driel: Phys. Rev. B **27** (1983) 1141.
2) J. F. Young, J. F. Preston, H. M. van Driel, and J. E. Sipe: Phys. Rev. B **27** (1983) 1155.
3) J. F. Young, J. E. Sipe, and H. M. van Driel: Phys. Rev. B **30** (1984) 2001.
4) S. Sakabe, M. Hashida, S. Tokita, S. Namba, and K. Okamuro: Phys. Rev. B **79** (2009) 033409.
5) J. Bonse, A. Rosenfeld, and J. Krüger: Appl. Surf. Sci. **257** (2011) 5420.
6) G. Miyaji and K. Miyazaki: Appl. Phys. Lett. **89** (2006) 191902.
7) A. Borowiec and H. K. Haugen: Appl. Phys. Lett. **82** (2003) 4462.
8) J. Bonse, S. Baudach, J. Krüger, W. Kautek, and M. Lenzner: Appl. Phys. A **74** (2002) 19.
9) T. H. R. Crawford and H. K. Haugen: Appl. Surf. Sci. **253** (2007) 4970.
10) D. Dufft, A. Rosenfeld, S. K. Das, R. Grunwald, and J. Bonse: J. Appl. Phys. **105** (2009) 034908.
11) R. Wagner, J. Gottmann, A. Horn, and E. W. Kreutz: Appl. Surf. Sci. **252** (2006) 8576.
12) B. Yu, P. Lu, N. Dai, Y. Li, X. Wang, Y. Wang, and Q. Zheng: J. Opt. A **10** (2008) 035301.
13) C. Teichert: Phys. Rep. **365** (2002) 335.
14) S. Kaneko, T. Ito, K. Akiyama, M. Yasui, C. Kato, S. Tanaka, Y. Hirabayashi, A. Mastuno, T. Nire, H. Funakubo, and M. Yoshimoto: Nanotechnology **22** (2011) 175307.
15) X. Wang, C. A. Ohlin, Q. Lu, and J. Hu: Biomaterials **29** (2008) 2049.
16) G. Obara, Y. Tanaka, N. N. Nedyalkov, M. Terakawa, and M. Obara: Appl. Phys. Lett. **99** (2011) 061106.
17) M. Huang, F. Zhao, Y. Cheng, N. Xu, and Z. Xu: ACS Nano **3** (2009) 4062.
18) T. Q. Jia, H. X. Chen, M. Huang, F. L. Zhao, J. R. Qiu, R. X. Li, Z. Z. Xu, X. K. He, J. Zhang, and H. Kuroda: Phys. Rev. B **72** (2005) 125429.
19) Q. Wu, Y. Ma, R. Fang, Y. Liao, Q. Yu, X. Chen, and K. Wang: Appl. Phys. Lett. **82** (2003) 1703.
20) F. Liang, R. Vallée, and S. L. Chin: Opt. Express **20** (2012) 4389.
21) J. Burghoff, S. Nolte, and A. Tünnermann: Appl. Phys. A **89** (2007) 127.
22) D. F. Nelson and R. M. Mikulyak: J. Appl. Phys. **45** (1974) 3688.
23) J. Lamela, G. Lifante, T. P. J. Han, F. Jaque, A. García-Navarro, J. Olivares, and F. Agulló-López: Appl. Surf. Sci. **255** (2009) 3918.
24) N. Bloembergen: Appl. Opt. **12** (1973) 661.
25) O. F. Schirmer, O. Thiemann, and M. Wöhlecke: J. Phys. Chem. Solids **52** (1991) 185.
26) J. R. Schwesyg, M. C. C. Kajiyama, M. Falk, D. H. Jundt, K. Buse, and M. M. Fejer: Appl. Phys. B **100** (2010) 109.
27) T. Suzuki: J. Mater. Sci. **30** (1995) 2873.
28) G. Obara, N. Maeda, T. Miyanishi, M. Terakawa, N. N. Nedyalkov, and M. Obara: Opt. Express **19** (2011) 19093.
29) M. Terakawa, S. Takeda, Y. Tanaka, G. Obara, T. Miyanishi, T. Sakai, T. Sumiyoshi, H. Sekita, M. Hasegawa, P. Viktorovitch, and M. Obara: Prog. Quantum Electron. **36** (2012) 194.